Rapid Communications

Giant thermally-enhanced electrostriction and polar surface phase in $La_2Mo_2O_9$ oxygen ion conductors

Qian Li,[1,2,*] Teng Lu,[3] Jason Schiemer,[4] Nouamane Laanait,[1] Nina Balke,[1] Zhan Zhang,[2] Yang Ren,[2] Michael A. Carpenter,[4] Haidan Wen,[2] Jiangyu Li,[5] Sergei V. Kalinin,[1] and Yun Liu[3,†]

[1]*Center for Nanophase Materials Sciences, Oak Ridge National Laboratory, Oak Ridge, Tennessee 37831, USA*

[2]*X-ray Science Division, Argonne National Laboratory, Lemont, Illinois 60439, USA*

[3]*Research School of Chemistry, The Australian National University, Canberra, ACT 0200, Australia*

[4]*Department of Earth Sciences, University of Cambridge, Cambridgeshire CB2 3EQ, United Kingdom*

[5]*Department of Mechanical Engineering, University of Washington, Seattle, Washington 98195, USA*

(Received 22 March 2018; published 27 April 2018)

Ferroelectrics possess spontaneous electric polarization at macroscopic scales which nonetheless imposes strict limitations on the material classes. Recent discoveries of untraditional symmetry-breaking phenomena in reduced material dimensions have indicated feasibilities to extend polar properties to broader types of materials, potentially opening up the freedom for designing materials with hybrid functionalities. Here, we report the unusual electromechanical properties of $La_2Mo_2O_9$ (LAMOX) oxygen ion conductors, systematically investigated at both bulk and surface length levels. We first observed giant electrostriction effects in $La_2Mo_2O_9$ bulk ceramics that are thermally enhanced in concert with their low-energy oxygen-vacancy hopping dynamics. Moreover, while no clear bulk polarization was detected, the surface phases of LAMOX were found to be manifestly polar, likely originating from the coupling between the intrinsic structural flexibilities with strain gradients (i.e., flexoelectricity) and/or chemical heterogeneities present in the materials. These findings identify $La_2Mo_2O_9$ as a promising electromechanical material system and suggest that the flexible structural and chemical configurations in ionically active materials could enable fundamentally different venues to accommodate electric polarization.

DOI: 10.1103/PhysRevMaterials.2.041403

Electromechanical materials used in modern actuating and sensing technologies have been dominated by ferroelectrics, whose spontaneous polarization generates linear-in-electric field strains; sometimes, the quadratic-in-field electrostriction effect is also utilized based on relaxors, akin to ferroelectrics [1–3]. Traditionally, ferroelectric polarization is understood as bulk phenomena restricted to noncentrosymmetric crystal structures. Recent material explorations have revealed intriguing polar phenomena in (bulk) centrosymmetric crystals under varying electromechanical and chemical boundary conditions. Of note are the recent reports of surface polar phases in paraelectric oxides including $SrTiO_3$, TiO_2, $BiVO_4$, and WO_3 [4–10], in the presence or absence of incipient polar instabilities. Despite the dearth of quantitative information on its strength and spatial extent, surface polarization in these materials has been shown to nontrivially influence other functionalities ranging from modulating electronic conductance [6,7] to enhancing photochemical reactivity [9,10]. While the unearthing of untraditional polar phenomena potentially has significant technological impact, elucidating their underlying mechanisms remains an active field of research. Most notably, mechanisms mediated by strain gradients (namely, flexoelectricty [11–13]) and chemical defects [5,8] have been proposed and extensively investigated. In this context, exploring the presence of surface polarization within the broader range of materials that are bulk paraelectrics, yet with a propensity to naturally host both strain and/or composition gradients, could shed invaluable information on the coupling behaviors between electric polarization and a system's structural, chemical, or electronic configurations [14].

$La_2Mo_2O_9$ and its derivatives (LAMOX) comprise a new family of oxygen ion conductors which contain intrinsic O vacancies without relying on aliovalent doping [15–19]. As shown in Fig. 1(a), the high-temperature β phase ($P2_13$ space group) has three unique O sites with the O2 and O3 sites partially occupied, leading to two O vacancies per unit cell and varying Mo coordination polyhedra. These structural characteristics of LAMOX are believed to host O-vacancy hopping mechanisms with very low activation energy barriers [16,17]. Pure LAMOX undergoes a ferroelastic phase transition at ~853 K and the resultant α phase ($P2_1$ space group) develops a $2 \times 3 \times 4$ superstructure with a long-range-ordered O sublattice [18]. Per these reported crystal structures, both phases are noncentrosymmetric, thus allowing piezoelectricity and the α phase can also be ferroelectric. However, theoretical analyses or first-principles calculations of the spontaneous polarization in the latter are hindered by its large unit cell containing 312 unique atoms [18], further complicated by the inherent propensity for O ion delocalization and local structure formation.

Here, we report on the unusual electromechanical behavior of LAMOX based on comprehensive structure and property characterizations. These materials are found to exhibit giant bulk electrostriction effects that can be enhanced at elevated

*qianli@anl.gov
†yun.liu@anu.edu.au

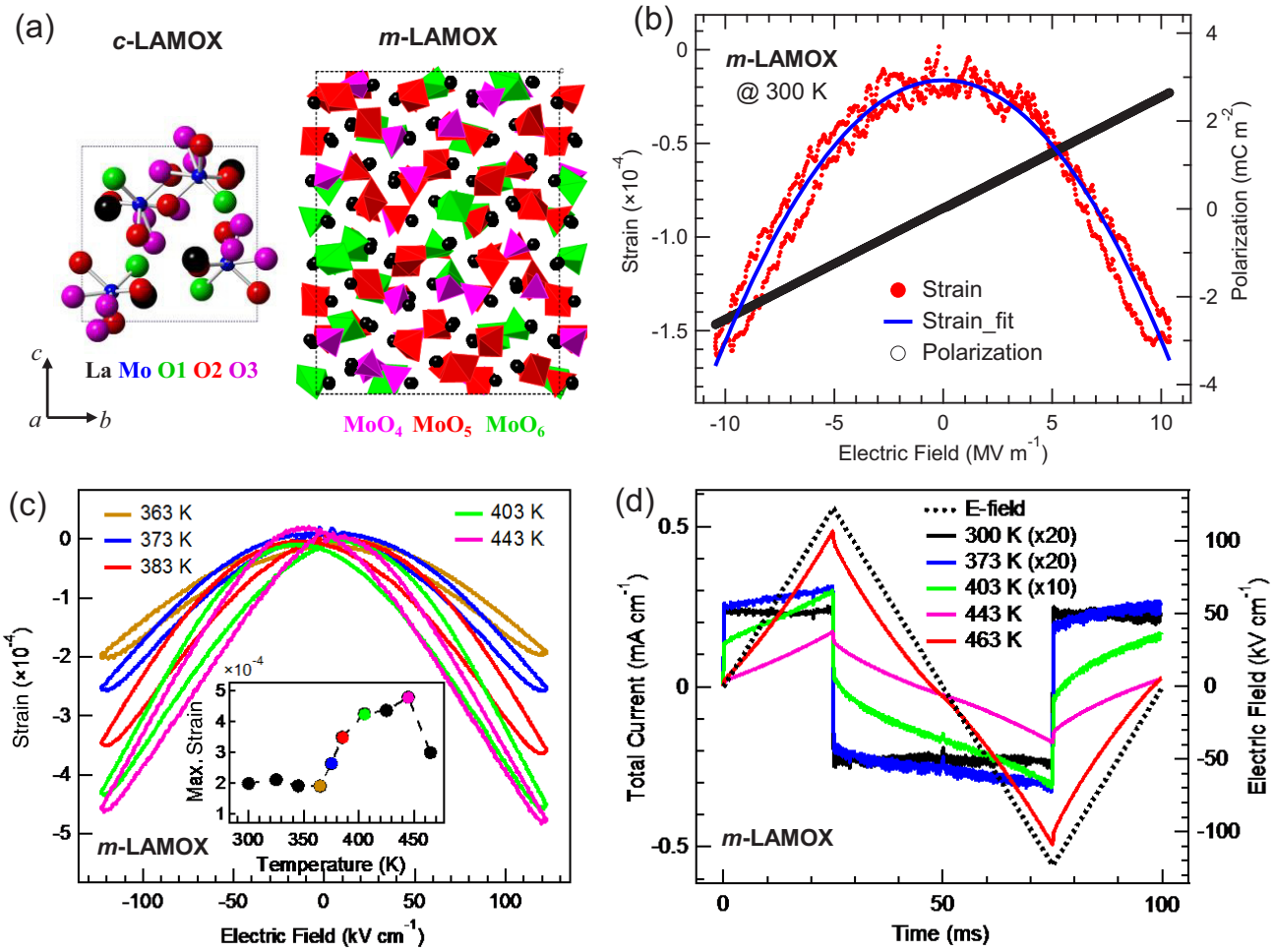

FIG. 1. (a) Crystal structures of m/c-LAMOX, viewed along the $[100]_C$ axis; note that their unit cells are not drawn in scale with the real lengths. (b) Typical P/S-E hysteresis loops of m-LAMOX, measured using a 10 Hz triangular wave form at 300 K, along with the quadratic fitting to the S-E loop. (c) S-E loops of m-LAMOX measured during heating; the inset shows the peak-to-tip strain value as a function of temperature. (d) Selected single-cycle total switching current loops of m-LAMOX, simultaneously measured with the strain loops in (c).

temperatures. It is further revealed that, despite the absence of measurable bulk polarization, the surface phases of LAMOX are manifestly polar and piezoelectric with grain/twin contrasts. All these results exhibit a compelling correlation with the oxygen vacancy configurations and hopping dynamics of the system and imply their inherent couplings. This Rapid Communication thus not only identifies a material family with hybrid electromechanical functionalities, but may suggest different routes to modulate polarization at meso/nanoscales in ionically active materials.

The materials studied are pure $La_2Mo_2O_9$ (monoclinic, hereafter denoted as m-LAMOX) and La_2MoWO_9 (cubic, c-LAMOX) in the form of polycrystalline ceramics; the latter was chosen as a proxy for the high-temperature β phase given that the isovalent W doping can suppress the β-α phase transition [19]. X-ray diffraction (XRD) and Raman spectroscopy confirm that m-LAMOX has a more distorted lattice symmetry than c-LAMOX as well as the occurrence of superstructures (see Fig. S1 in the Supplemental Material [20]). Figure 1(b) illustrates typical bulk polarization and strain versus electric field (P/S-E) loops measured for m-LAMOX at ~300 K. The P-E loops are linear and essentially hysteresis free, indicating ideal dielectric behavior with a relative permittivity $\varepsilon \sim 28$ and absence of switchable polarization under an E field of 100 kV cm^{-1}. Correspondingly, the S-E loops exhibit a quadratic relationship between the longitudinal strain (note the negative sign) and applied E field due to an electrostriction effect. Fitting the measured strains to the quadratic model (see the Methods section in the Supplemental Material [20]) yields a longitudinal electrostriction coefficient $M \sim -1.5 \times 10^{-18}$ m^2 V^{-2} or $Q \sim 20$ m^4 C^{-2} as well as a negligible piezoelectric coefficient $d \sim 0.03$ pm V^{-1}. This again implies that no appreciable spontaneous polarization (P_s) is present in bulk m-LAMOX, since otherwise it would produce a linear strain response in proportion to $2\varepsilon Q P_s E$ [3]. For c-LAMOX, similar P/S-E loop behavior was observed with a higher $\varepsilon_r \sim 48$ and slightly lower $M \sim -1.3 \times 10^{-18}$ m^2 V^{-2} [Figs. S2(a) and S2(b) [20]]. These electrostriction coefficients of LAMOX are in the same order of magnitude as those recently reported for doped CeO_2 and δ-Bi_2O_3 O ion conductors [21–23] and much larger than most other inorganic solids, for example, $M \sim 10^{-22}$ m^2 V^{-2} of SiO_2 and $Q \sim 10^{-2}$ m^4 C^{-2} of $Pb(Mg_{1/3}Nb_{2/3})O_3$, a classical electrostrictor [2].

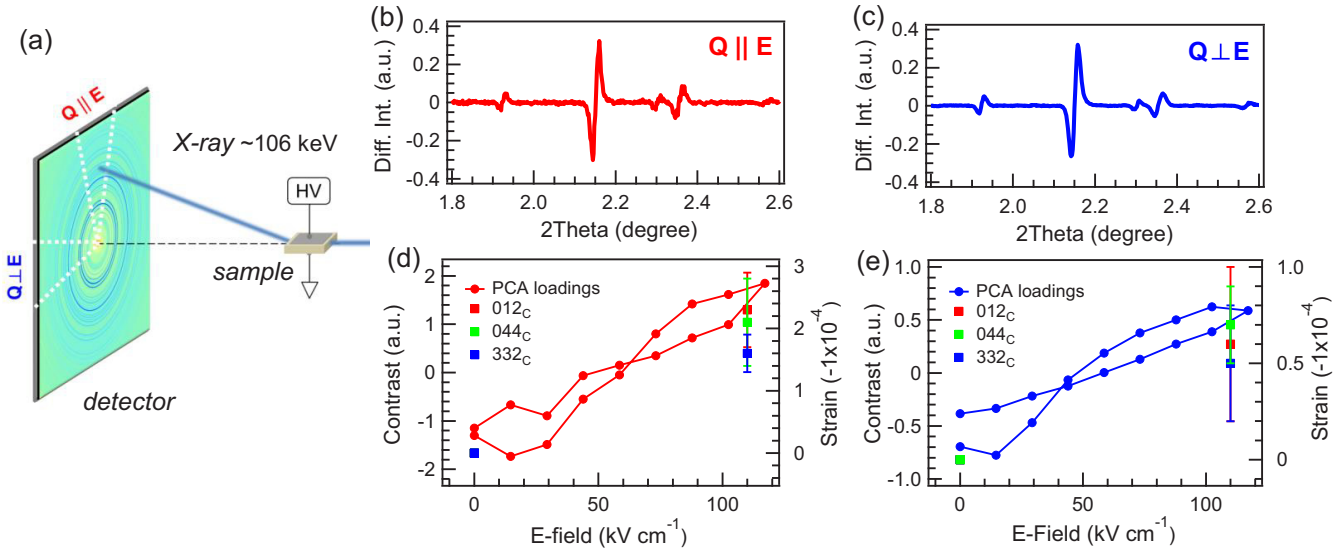

FIG. 2. (a) Schematic for the *in situ* high-energy XRD setup. (b), (c) The eigenvectors and (d), (e) loadings of the second principal components of the diffraction patterns measured along the (b), (d) parallel-to-field and (c), (e) transverse-to-field directions. Also shown in (d) and (e) are the absolute lattice strains at the highest E field (slightly offset for clarity) relative to zero field. These strains were calculated from fittings to selected Bragg peaks as labeled with the cubic phase indices, and the error bars denote the fitting uncertainties.

We then performed heating P/S-E loop measurements up to ~473 K. Figure 1(c) shows the S-E loops of m-LAMOX for selected temperatures and the peak-to-tip values of E-field-induced strains compiled from all the loops (see the inset). The parabola, no-hysteresis loop characters appear to be largely unaltered by heating, with only the loops at the highest temperatures becoming slightly straight. More remarkably, the measured strain response increases steadily above ~370 K and reaches a maximum value of ~0.05% at 443 K. This latter strain, generated by the quadratic coupling effect under ~120 kV cm^{-1}, equates to a linearized coupling effect with a sizable coefficient of −40 pm V^{-1}. With increasing temperature, the corresponding P-E loops exhibit a larger in-phase resistive (versus capacitive) component, which starts to dominate the total switching current at ~423 K [Fig. 1(d)]. Note that the strain response is still observed to increase somewhat above 423 K. At present, the exact mechanistic relationship between the conducting current and electrostrictive strain is unclear; nonetheless, a significantly lossy behavior seen at 463 K may well relate to the onset of falling strain response therein. Likewise, c-LAMOX also shows an increasing behavior in the temperature-dependent P/S-E loops, albeit with a smaller and more gradual increase in both measured strains and conducting current (see Fig. S2 [20]).

We have confirmed the electrostriction response for m-LAMOX at 300 K using *in situ* high-energy XRD [see Fig. 2(a)]. Here, to quickly (while qualitatively) extract the main trends of E-field-induced changes, we analyzed the diffraction patterns using a statistical method, principal component analysis (PCA) [24]. In brief, PCA finds a set of orthogonal, linearly uncorrelated eigenvectors or components and decomposes the original data set onto those eigenvectors in such a way that the resultant components are arranged according to their variance or relative importance. The use of PCA also virtually enhances the strain resolution (~10^{-4}) of our instrument.

The acquired data set was found to contain two principal components, the first one largely being due to the beam flux fluctuations (see Fig. S3 [20]). The second eigenvectors show systematical oscillations that correspond to differential intensity signals due to lattice strains. As illustrated in Figs. 2(b) and 2(c), these signals, for both parallel- and transverse-to-field cases, consist of negative-to-positive transitions at all reflections, meaning their peak shifts towards higher angles, namely, lattice contraction. The loadings (weights) of the second component, plotted as unipolar E-field loops in Figs. 2(d) and 2(e), show monotonic increasing trends with small hysteresis, well corroborating the measured (longitudinal) bulk S-E loops. Note that the transverse-to-field direction exhibits negative lattice strains as well, indicating negative transverse electrostriction coefficients and thus a volumetric field-induced contraction effect. The absolute lattice strains are calculated to be ~0.02% (longitudinal) at 115 kV cm^{-1} [overlaid on Figs. 2(d) and 2(e)], in quantitative agreement with the aforementioned polycrystalline-averaged bulk strains.

To gain more insights into the bulk electromechanical behavior of LAMOX, we resorted to two types of ultrasonic elastic techniques (see the Methods section in the Supplemental Material for details [20]). The first is resonant piezoelectric spectroscopy (RPS), which is highly sensitive to the presence of electric polarization and has been used to probe polar twin walls in nonpolar $SrTiO_3$ and nanosized polar precursors in the paraelectric phase of $BaTiO_3$ [25,26]. Also, there is a noteworthy difference between RPS and the P/S-E loops in that the latter measurement only evaluates switchable polarization. As shown in Fig. 3(a), the acquired RPS spectra of m-LAMOX only consist of a slowly-varying background without any detectable first-harmonic resonance signals that would arise from polarization in response to the ac excitation electric fields. By contrast, c-LAMOX does show several traces of weak resonance (indicated by the arrows) under the same measuring conditions. Such results are rather unexpected and

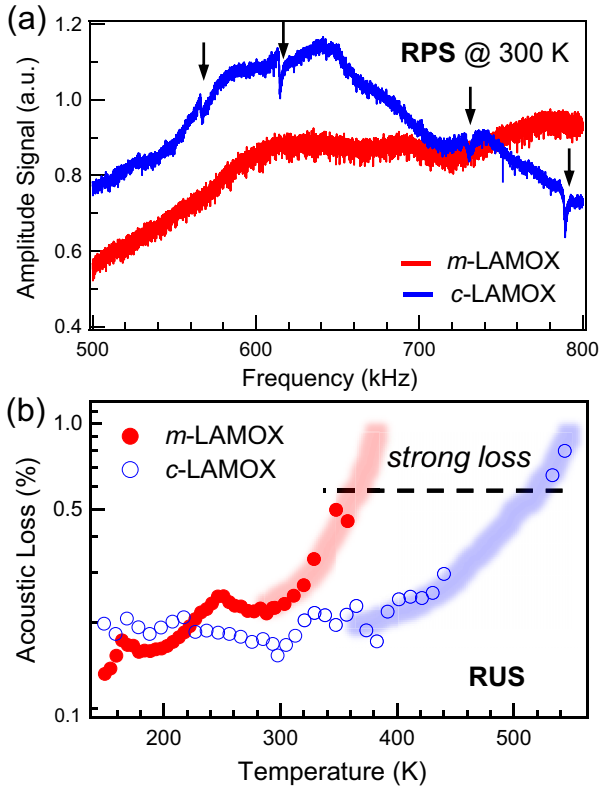

FIG. 3. (a) RPS frequency response spectra (portion) of m/c-LAMOX. The m-LAMOX signal is multiplied by a factor of 2. The arrows denote the detected resonance peaks. (b) Temperature evolution of the acoustic loss factor of m/c-LAMOX, derived by Lorentzian fittings to the measured RUS resonance peaks. The dashed line denotes the strong-loss regime, where a reliable determination of the loss factor was unfeasible. The shadow lines are a guide to eye.

contradictory to their average crystal structure symmetries; c-LAMOX belongs to a nonpolar space group and is evidently less distorted than m-LAMOX in the bulk phase. Therefore, RPS confirms the otherwise nonpolar bulk nature of both m/c-LAMOX while suggesting the likely presence of localized polarization unrestricted by the average crystal structures.

The other ultrasonic method, resonant ultrasound spectroscopy (RUS), directly probes the (an)elasticity of LAMOX. The anelastic behavior in oxygen ion conductors commonly stems from the relaxation of elastic dipoles formed by O vacancies and correlates with their O ion hopping dynamics [27–29]. Figure 3(b) depicts the evolution of the acoustic loss factor (fitted from the RUS resonance peaks; see the raw spectra in Fig. S4 [20]) over a wide temperature range. Overall, LAMOX shows complex anelastic behavior, as indicated by the kinks at several temperatures, suggesting a cooperation of multiple coexistent O-vacancy hopping processes. Focusing on the same temperature interval as the P/S-E loops, an onset of strong acoustic loss (which renders the resonance peaks heavily damped) accompanied with elastic softening is observed around ∼360 K in m-LAMOX, whereas a similar onset appears to occur at least 100 K higher in c-LAMOX, indicating a larger energy barrier to overcome. Note that such a difference may corroborate previous studies which showed suppressed ion migration activities by W doping [22] and perhaps also our conducting current (P-E loop) results. The onset temperature in the acoustic loss coincides well with the observed enhancement of electrostrictive strain above ∼370 K in m-LAMOX, which naturally points to a shared activation mechanism presumably associated with the low-energy O-vacancy hopping processes.

These bulk measurement results raise questions about the surface properties of LAMOX; in particular, the fact that high-symmetry c-LAMOX shows finite RPS signals strongly implies divergent electromechanical behavior in the surface phases. To examine this over a length scale of a few tens nanometers, piezoresponse force microscopy (PFM) was performed [30,31]. Figures 4(a) and 4(b) show the piezoresponse images of m/c-LAMOX (amplitude and phase combined; note the absence of 180°-phase flips or sign changes) acquired using the same calibrated PFM probe at ∼300 K. For both materials, a small (∼0.5−3 pm/V) yet clearly distinguishable surface piezoresponse can be quantitatively probed with contact-resonance-enhanced PFM techniques [32]. The PFM image of c-LAMOX exhibits a weak grain contrast in accordance with the grain orientation map [Fig. 4(c)] obtained from site-correlated electron backscattering diffraction (EBSD) measurements. By contrast, the PFM image of m-LAMOX not only shows this grain contrast [see the overlaid grain contours in Fig. 4(a)], but, more strikingly, reveals a wealth of subgrain features that are entirely absent on the EBSD orientation map or topography (not shown). These features can be attributed to the ferroelastic twin structure of m-LAMOX, which in principle can consist of six twin variants with the $\langle 001\rangle_C$-type (in the cubic phase indices) spontaneous shear strains separated by the $\{001\}_C$-type twin walls. We have confirmed this twin structure using full-field x-ray diffraction microscopy [33]. Figure 4(d) illustrates the diffraction contrast of a grain that overall satisfied the 021_C Bragg conditions. Due to having different lattice tilts/strains, various parts of the grain became optimally aligned, thereby showing maximum intensities at different rocking angles. These revealed subgrain structural features exhibit close similarities with the piezoresponse domains in both their lateral spatial extent and configurations across the grains.

The observation of a surface piezoresponse in LAMOX *per se* is significant, given no linear response detected at the bulk level. Here, the revealed twin/grain contrast provides the means to distinguish various plausible PFM signal generation mechanisms. First, it can be readily verified that the recorded signals are electromechanical in nature with minimal electrostatic contribution [34], since the surface charge distribution on both samples is featureless, as imaged by Kelvin probe force microscopy [see Figs. S5(a) and S5(b) [20]]. We further probed local elastic stiffness via atomic force acoustic microscopy [35] and found only grain contrast but no twin contrast in m-LAMOX [see Figs. S5(d) and S5(e) [20]], thus ruling out contrast mechanisms arising from dissimilar elastic properties. Moreover, the contribution of bulk piezoelectricity to the PFM signals can be ruled out by analyzing their orientation dependence. For simplicity, consider the case of c-LAMOX whose $P2_13$ symmetry only allows nonzero d_{14} coefficients, resulting in a longitudinal piezoelectric effect that is maximum along $\langle 111\rangle_C$ and vanishes along $\langle 001\rangle_C$ and $\langle 110\rangle_C$ [see the tensor surface in Fig. S5(f) [20]] [36]. The PFM signals are generally known to correlate to the longitudinal piezoelectric

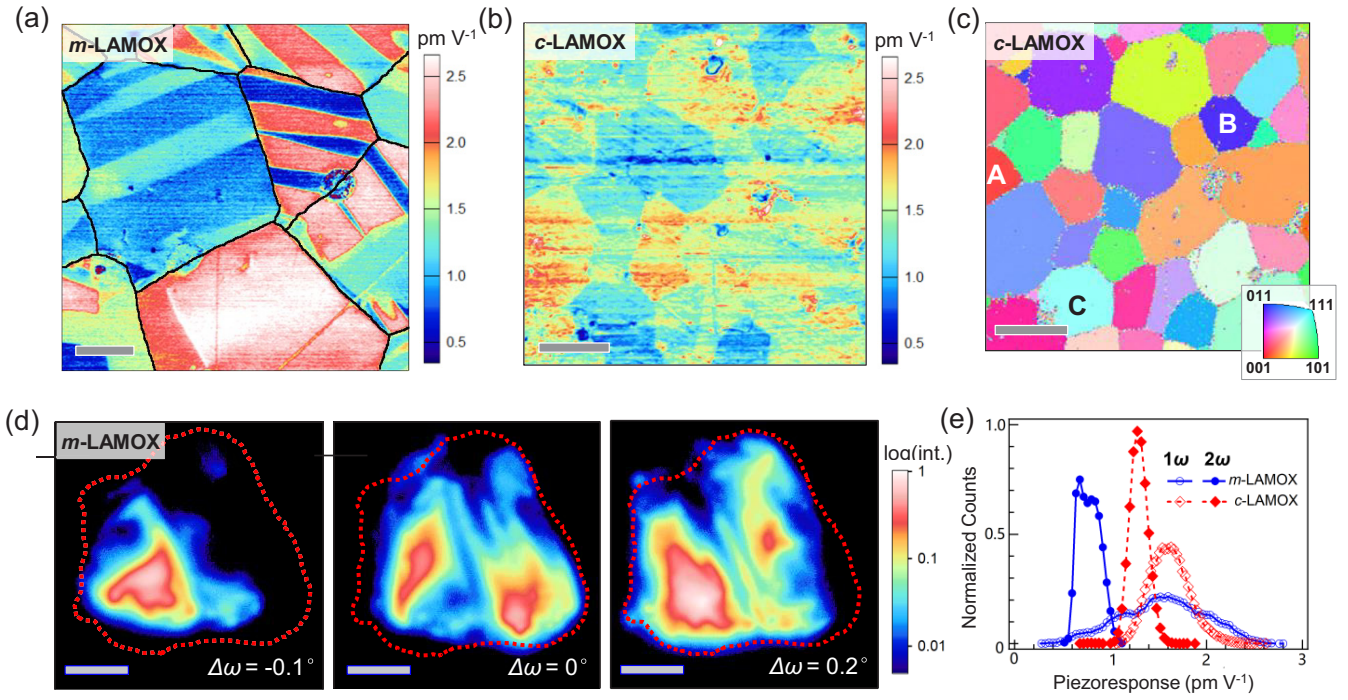

FIG. 4. Typical PFM images of (a) m-LAMOX and (b) c-LAMOX acquired at 300 K. (c) EBSD orientation map of c-LAMOX from the same site as (b). Grains marked as A, B, and C correspond to surface normal orientations close to $\langle 001\rangle_C$, $\langle 110\rangle_C$, and $\langle 111\rangle_C$, respectively. The EBSD-derived grain-boundary contour of m-LAMOX is overlaid in (a). (d) Selected full-field x-ray diffraction microscopy images of a single m-LAMOX grain, taken at different ω rocking angles based on the 021_C Bragg condition. The dashed lines indicate the projected grain boundary. The scale bar is 1 μm in (a), (d) and 5 μm in (b), (c). (e) Histograms of the 1ω and 2ω piezoresponse images, measured at the same regions in m/c-LAMOX.

effect and thus should follow its orientation dependence if such an effect were dominant. Instead, minimal piezoresponse variations exist on c-LAMOX grains with (close to) the above special orientations [see grains A, B, and C in Fig. 4(c); cf. Fig. 4(b)]. In essence, PFM confirms that LAMOX has negligibly small bulk piezoelectricity, in corroboration with the S-E loop results.

All the above results consistently point to the fact that the surfaces of our LAMOX materials are polar to a certain extent. The occurrence of surface spontaneous polarization (P_s^S) couples with electrostriction, thereby generating a linear response with a coefficient of $2\varepsilon Q P_s^S$, as detected by standard first-harmonic (1ω) PFM. The collective response of these polar surface phases over the whole m/c-LAMOX samples also appears to be the most likely origin of the acquired RPS signals. From an average piezoresponse of a few pm V^{-1}, P_s^S can be estimated to be around $0.1-1$ mC m^{-2} (ε and Q are known). Besides, as with the bulk S-E loop measurements, the quadratic electrostriction coupling component $Q(\varepsilon E)^2$ can be detected in the form of second-harmonic (2ω) PFM signals. Comparing the 1ω and 2ω piezoresponses thus can factor out the dependence of Q and provide additional clues about the magnitude of P_s^S in LAMOX. Figure 4(e) shows the histograms of the two types of PFM images acquired using the same ac excitation voltages. For both materials, the 1ω and 2ω piezoresponses are quantitatively comparable, in marked contrast with typical ferroelectrics which have $0.01-1$ C m^{-2} bulk polarizations and accordingly exhibit a predominantly linear response [37]. This comparison thus reinforces our estimated value of the surface polarization.

Further evidence for the electrostrictive nature of the surface piezoresponses in LAMOX is present in their temperature behavior as measured by *in situ* heating PFM. Figure 5 shows the calibrated and spatially averaged piezoresponses for m/c-LAMOX as a function of temperature. Compared with traditional ferroelectrics including $Pb(Zr,Ti)O_3$ and $BiFeO_3$ [38], LAMOX exhibits a much more pronounced increase in piezoresponse at elevated temperatures. Remarkably, this increasing trend of m-LAMOX is found to consist of two distinct regimes with a crossover occurring at ~370 K, which is consistent with both "transition temperatures" shown in the S-E loop and RUS results. And again, c-LAMOX exhibits a singular, slowly increasing trend over the same temperature range. Hence these trends suggest that the observed piezoresponse enhancement is primarily due to the thermally enhanced bulk electrostriction properties. Concomitant reconfigurations of the surface polarization may also likely occur upon heating, as reflected by the gradually weakened twin contrast [see Fig. 5(a)]. Furthermore, we fit the acquired piezoresponse data to the Arrhenius model [39], obtaining an activation energy of ~0.3 eV for the above-370-K regime of m-LAMOX and ~0.1 eV for its low-temperature regime as well as the whole range measured for c-LAMOX. These values fall well within the theoretical and x-ray diffraction-derived energy scales for the intra-MoO_x polyhedra O-vacancy hopping barriers associated with the O2 and O3 sites (which are ~0.15 and ~0.57 eV,

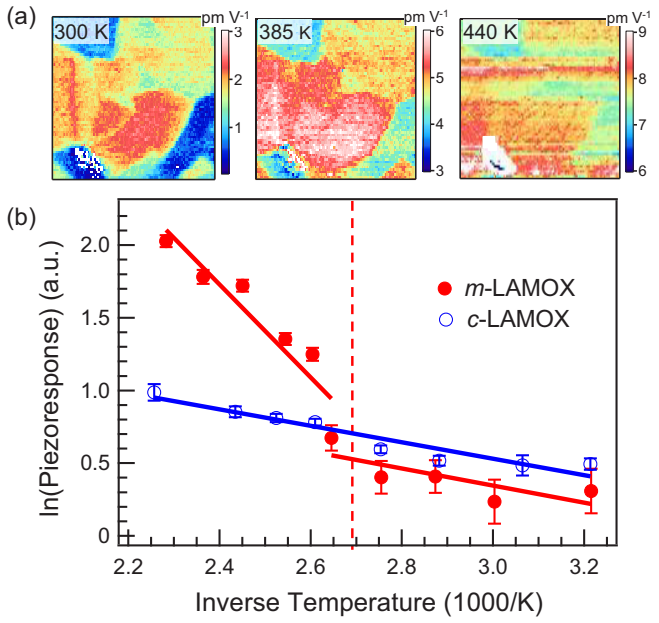

FIG. 5. (a) PFM images of m-LAMOX measured at selected heating temperatures. Image size: $2 \times 2\,\mu\mathrm{m}^2$. (b) Image-averaged piezoresponse of m/c-LAMOX as a function of inverse temperature. The lines are the Arrhenius fittings to each temperature regime. The error bars denote the variations of piezoresponse over the whole images.

respectively [16,17]), thus implying the microscopic basis for the electrostriction response.

The uncovering of giant electrostriction effects in LAMOX illustrates the electromechanical properties of O ion conductors that potentially rival known lead-free ferroelectric systems [40], in resonance with Lubomirsky *et al.*'s recent reports on doped CeO_2 and δ-Bi_2O_3 [21,22]. These authors proposed three guidelines for searching other materials: fluorite structure, the presence of O vacancies, and anelastic behavior. Apparently, our results have expanded the material structures while attesting to the latter two criteria. In light of the mechanisms they proposed for ceria, we infer that the electrostrictive coupling in LAMOX stems from a local rearrangement of O-vacancy elastic dipoles under applied E fields, which very likely hinges on the intra-MoO_x hopping processes. This mechanism is compellingly corroborated by the multiple consistent thermal activation behaviors revealed by several distinct techniques (S-E loop, RUS, and PFM). The activated O-vacancy dynamics can facilitate the field-induced elastic dipole rearrangement, leading to enhanced strain couplings; however, in the overly activated regime (e.g., m-LAMOX at 463 K) the long-range, inter-MoO_x migration of O vacancies may become significant and adversely affect the electrostriction properties. We anticipate more microscopic insights to be gained in future studies incorporating local probes, such as *in situ* extended x-ray absorption fine structure, though invariably challenging due to the structural intricacies.

The polar surface phases in our LAMOX samples could be of somewhat extrinsic structural origins. Flexoelectricity, that is, strain-gradient-induced lattice symmetry breaking as described by the constitutive equation $P = \varepsilon f\, \partial e/\partial x$ (where e is strain and f the flexocoupling coefficient), can be an important polarization effect here. Given that f is typically 1–10 V for inorganic crystalline materials [13,24], we estimate strain gradients $\sim 10^5 - 10^6\ \mathrm{m}^{-1}$ that would be responsible for the $0.1-1\ \mathrm{mC\,m}^{-2}$ surface polarization as derived from the PFM results. Such strain gradient levels can be reasonably expected to develop along the surface depth profiles during the fabrication processes [4,41]. Besides, the spontaneous strains in m-LAMOX can only be partially relaxed towards the surface [9,10], bringing in an additional source of strain gradient that modulates the surface polarization and piezoresponse. Another possible origin of polarization can arise from an inhomogeneous distribution of O vacancies near the surface, essentially a space-charge effect [39]. Still, this latter effect can coact with flexoelectricity since lattice strains are usually accompanied with defects in oxides [5]. In any case, the high structural flexibilities of LAMOX may have provided the key microscopic basis to host local structures that are more polarized in the surface phase than the bulk average.

From a phenomenological viewpoint, enhancing electric polarization via the strain gradient effect may provide a practical approach to leverage the electrostriction properties of LAMOX. This can be realized by using well-established strain and interface-engineering thin-film techniques [42] (e.g., over $10^6\ \mathrm{m}^{-1}$ strain gradients obtained in $BiFeO_3$ thin films in Ref. [43]), and through reducing the dimensions of these materials, a convergence in the bulk and surface electromechanical response would result. Tuning the electrostriction and polarization properties of LAMOX can also be envisaged by using chemical doping routes to modify the oxygen-vacancy configurations and hopping behaviors. Our findings thus suggest that $La_2Mo_2O_9$ and alike compounds comprise promising types of electromechanical materials with the potential to host large functional tunability and flexibility.

Q.L. and H.W. were supported by the US Department of Energy, Office of Science, Materials Science and Engineering Division. T.L. and Y.L. acknowledge the support of the Australian Research Council (ARC) in the form of Discovery Projects (DP160104780). N.L. was supported by the Eugene P. Wigner Fellowship program at ORNL (No. DE-AC05-00OR22725). The PFM experiments were performed at the Center for Nanophase Materials Sciences, which is a DOE Office of Science User Facility at Oak Ridge National Laboratory (ORNL). The use of Advanced Photon Source was supported by the US DOE, Basic Energy Science under Contract No. DE-AC02-06CH11357.

[1] V. Sundar and R. E. Newnham, Ferroelectrics **135**, 431 (1992).

[2] R. E. Newnham, V. Sundar, R. Yimnirun, J. Su, and Q. M. Zhang, J. Phys. Chem. B **101**, 10141 (1997).

[3] F. Li, L. Jin, Z. Xu, and S. Zhang, Appl. Phys. Rev. **1**, 011103 (2014).

[4] A. Kholkin, I. Bdikin, T. Ostapchuk, and J. Petzelt, Appl. Phys. Lett. **93**, 222905 (2008).

[5] Y. Kim, A. N. Morozovska, A. Kumar, S. Jesse, E. A. Eliseev, F. Alibart, D. Strukov, and S. V. Kalinin, ACS Nano **6**, 7026 (2012).

[6] C. W. Bark, P. Sharma, Y. Wang, S. H. Baek, S. Lee, S. Ryu, C. M. Folkman, T. R. Paudel, A. Kumar, S. V. Kalinin, A. Sokolov, E. Y. Tsymbal, M. S. Rzchowski, A. Gruverman, and C. B. Eom, Nano Lett. **12**, 1765 (2012).

[7] P. Sharma, S. Ryu, J. D. Burton, T. R. Paudel, C. W. Bark, Z. Huang, Ariando, E. Y. Tsymbal, G. Catalan, C. B. Eom, and A. Gruverman, Nano Lett. **15**, 3547 (2015).

[8] D. Lee, H. Lu, Y. Gu, S.-Y. Choi, S.-D. Li, S. Ryu, T. R. Paudel, K. Song, E. Mikheev, S. Lee, S. Stemmer, D. A. Tenne, S. H. Oh, E. Y. Tsymbal, X. Wu, L.-Q. Chen, A. Gruverman, and C. B. Eom, Science **349**, 1314 (2015).

[9] R. Munprom, P. A. Salvador, and G. S. Rohrer, Chem. Mater. **26**, 2774 (2014).

[10] A. S. Pisat, G. S. Rohrer, and P. A. Salvador, J. Mater. Chem. A **5**, 8261 (2017).

[11] P. Zubko, G. Catalan, A. Buckley, P. R. L. Welche, and J. F. Scott, Phys. Rev. Lett. **99**, 167601 (2007).

[12] J. F. Scott, J. Phys.: Condens. Matter **25**, 331001 (2013).

[13] P. V. Yudin and A. K. Tagantsev, Nanotechnology **24**, 432001 (2013).

[14] S. V. Kalinin and N. A. Spaldin, Science **341**, 858 (2013).

[15] P. Lacorre, F. Goutenoire, O. Bohnke, R. Retoux, and Y. Laligant, Nature (London) **404**, 856 (2000).

[16] C. J. Hou, Y. D. Li, P. J. Wang, C. S. Liu, X. P. Wang, Q. F. Fang, and D. Y. Sun, Phys. Rev. B **76**, 014104 (2007).

[17] A. M. Antipin, O. A. Alekseeva, N. I. Sorokina, A. N. Kuskova, M. Y. Presniakov, E. P. Kharitonova, and V. I. Voronkova, Acta Crystallogr., Sect. A **70**, 669 (2014).

[18] I. R. Evans, J. A. K. Howard, and J. S. O. Evans, Chem. Mater. **17**, 4074 (2005).

[19] S. Georges, O. Bohnke, F. Goutenoire, Y. Laligant, J. Fouletier, and P. Lacorre, Solid State Ionics **177**, 1715 (2006).

[20] See Supplemental Material at http://link.aps.org/supplemental/10.1103/PhysRevMaterials.2.041403 for experimental methods and additional XRD, Raman, P/S-E, RUS, PFM, and other AFM measurement results and analyses.

[21] R. Korobko, A. Patlolla, A. Kossoy, E. Wachtel, H. L. Tuller, A. I. Frenkel, and I. Lubomirsky, Adv. Mater. **24**, 5857 (2012).

[22] N. Yavo, A. D. Smith, O. Yeheskel, S. Cohen, R. Korobko, E. Wachtel, P. R. Slater, and I. Lubomirsky, Adv. Funct. Mater. **26**, 1138 (2016).

[23] A. D. Ushakov, E. Mishuk, E. Makagon, D. O. Alikin, A. A. Esin, I. S. Baturin, A. Tselev, V. Ya. Shur, I. Lubomirsky, and A. L. Kholkin, Appl. Phys. Lett. **110**, 142902 (2017).

[24] Q. Li, C. T. Nelson, S. L. Hsu, A. R. Damodaran, L. L. Li, A. K. Yadav, M. McCarter, L. W. Martin, R. Ramesh, and S. V. Kalinin, Nat. Commun. **8**, 1468 (2017).

[25] E. K. H. Salje, O. Aktas, M. A. Carpenter, V. V. Laguta, and J. F. Scott, Phys. Rev. Lett. **111**, 247603 (2013).

[26] O. Aktas, M. A. Carpenter, and E. K. H. Salje, Appl. Phys. Lett. **103**, 142902 (2013).

[27] R. Korobko, S. K. Kim, S. Kim, S. R. Cohen, E. Wachtel, and I. Lubomirsky, Adv. Funct. Mater. **23**, 6076 (2013).

[28] J. A. Schiemer, R. L. Withers, Y. Liu, and M. A. Carpenter, Chem. Mater. **25**, 4436 (2013).

[29] X. P. Wang and Q. F. Fang, Phys. Rev. B **65**, 064304 (2002).

[30] S. V. Kalinin, A. N. Morozovska, L.-Q. Chen, and B. J. Rodriguez, Rep. Prog. Phys. **73**, 056502 (2010).

[31] J. Li, J.-F. Li, Q. Yu, Q. N. Chen, and S. Xie, J. Materiomics **1**, 3 (2015).

[32] Q. Li, S. Jesse, A. Tselev. L. Collins, P. Yu, I. Kravchenko, S. V. Kalinin, and N. Balke, ACS Nano **9**, 1848 (2015).

[33] N. Laanait, Z. Zhang, C. M. Schleputz, J. Vila-Comamala, M. J. Highland, and P. Fenter, J. Synchrotron Radiat. **21**, 1252 (2014).

[34] S. V. Kalinin and D. A. Bonnell, Phys. Rev. B **65**, 125408 (2002).

[35] Q. Li, Y. Cao, P. Yu, R. K. Vasudevan, N. Laanait, A. Tselev, F. Xue, L.-Q. Chen, P. Maksymovych, and S. V. Kalinin, Nat. Commun. **6**, 8985 (2015).

[36] R. Newnham, *Properties of Materials Anisotropy, Symmetry, Structure* (Oxford University Press, Oxford, U.K., 2005).

[37] Q. N. Chen, Y. Ou, F. Ma, and J. Li, Appl. Phys. Lett. **104**, 242907 (2014).

[38] N. Balke, S. Kalnaus, N. J. Dudney, C. Daniel, S. Jesse, and S. V. Kalinin, Nano Lett. **12**, 3399 (2012).

[39] Q. N. Chen, S. B. Adler, and J. Li, Appl. Phys. Lett. **105**, 201602 (2014).

[40] J. Rödel, W. Jo, K. T. P. Seifert, E.-M. Anton, T. Granzow, and D. Damjanovic, J. Am. Ceram. Soc. **92**, 1153 (2009).

[41] A. Biancoli, C. M. Fancher, J. L. Jones, and D. Damjanovic, Nat. Mater. **14**, 224 (2015).

[42] L. W. Martin and A. M. Rappe, Nat. Rev. Mater. **2**, 16087 (2016).

[43] Y. L. Tang, Y. L. Zhu, Y. Liu, Y. J. Wang, and X. L. Ma, Nat. Commun. **8**, 15994 (2017).